

# Turbulent transport of MeV range cyclotron heated minorities as compared to alpha particles

István Pusztai<sup>1</sup>, George J. Wilkie<sup>1,2</sup>, Yevgen O. Kazakov<sup>3</sup> and Tünde Fülöp<sup>1</sup>

<sup>1</sup> Department of Physics, Chalmers University of Technology, SE-41296 Göteborg, Sweden

<sup>2</sup> Institute for Research in Electronics and Applied Physics, University of Maryland, College Park, MD 20742, USA

<sup>3</sup> Laboratory for Plasma Physics, LPP-ERM/KMS, 1000 Brussels, Belgium

E-mail: [pusztai@chalmers.se](mailto:pusztai@chalmers.se)

## Abstract.

We study the turbulent transport of an ion cyclotron resonance heated (ICRH), MeV range minority ion species in tokamak plasmas. Such highly energetic minorities, which can be produced in the three ion minority heating scheme [Ye. O. Kazakov et al. (2015) *Nucl. Fusion* **55**, 032001], have been proposed to be used to experimentally study the confinement properties of fast ions without the generation of fusion alphas. We compare the turbulent transport properties of ICRH ions with that of fusion born alpha particles. Our theoretical predictions indicate that care must be taken when conclusions are drawn from experimental results: While the effect of turbulence on these particles is similar in terms of transport coefficients, differences in their distribution functions – ultimately their generation processes – make the resulting turbulent fluxes different.

## 1. Introduction

The success of the magnetic confinement approach to fusion strongly relies on the confinement and transport of the alpha particles over the whole energy range from 3.5 MeV to the thermalized ash. These particles represent the source of heat for the self-sustained fusion reaction, they can damage the plasma facing components if they get lost before slowing down, and they can dilute the plasma if they would not leave the core after depositing their energy. Accordingly, a significant theoretical and experimental effort has been dedicated to the study of alpha particle physics [1, 2].

The ITER experiment is expected to demonstrate dominant alpha heating for the first time. In order to gain confidence in our capabilities to predict the behavior of alphas, various experiments and proposals considered mimicking alpha particles using energetic ion species from neutral beams and/or radio frequency (RF) heating (see for instance [3, 4]). Similarity scaling arguments can provide a guidance for such experiments to be relevant for alpha physics in reactor scale devices [4, 5, 6, 7]. Previous works have mostly been concerned with creating ITER-relevant situations in devices of smaller dimensions. Since ITER will operate in a non-activated mode for several years before starting to generate alphas in deuterium-tritium (DT) plasmas, it is instructive to consider possibilities to mimic alpha particles in scenarios which can be applied on ITER itself. For such experiments the generation of energetic ions in the MeV range would be desirable, which is not trivial to achieve using conventional heating techniques. In this paper we theoretically demonstrate that certain aspects of the *turbulent* transport of alpha particles may be studied already in the non-activated phase through generating very energetic trace minority ions by a novel ion cyclotron resonance heating (ICRH) scheme, while care must be taken with the interpretation of any experimental results because of the different nature of these species.

In this paper we only consider tokamaks, where, due to the almost perfect toroidal symmetry the vast majority of collisionless orbits are confined. Imperfections in toroidal symmetry can lead to direct orbit losses; it is a well understood process that can be effectively mitigated using ferritic steel inserts [8]. Fast particle driven instabilities – in particular various Alfvénic Eigenmodes (AE) – have been playing a major role in energetic particle losses in current tokamak experiments, and accordingly, they have received considerable attention (see recent reviews in Refs. [9, 10]). The importance of AEs in ITER is still an open question; a recent study [11] concludes that AE-induced transport is not expected to play a major role below mid-radius in a typical ITER scenario (due to the Landau damping being stronger than the fast particle drive). In any case, in a reactor the energetic alpha particle losses need to be kept within some tolerable level and for the majority of the alpha particles the collisional slowing down should happen on a flux surface; in this paper we assume this to be the case.

The effect of turbulence on fast ions is suppressed by finite Larmor radius (FLR) effects at very high energies. However, as pointed out in e.g. Ref. [12], across some

suprathermal energy range turbulence can play a major role in radially transporting alpha particles; in particular, the radial turbulent transport timescale can be much shorter than the slowing-down timescale. Thereby the energy distribution of alphas may be modified from the usually assumed slowing down distribution [13, 14, 15].

The energetic species that is used to mimic alphas should optimally reach temperatures well above the critical energy for electron drag to dominate the collisional slowing down [4]. There have been experimental studies generating high-energy ions to simulate fusion-born alpha particles. For instance, a neutral beam injection hot ion population of  $^4\text{He}$  was further energized from the 100 keV to the MeV range using third harmonic ICRH [3]. Recently, another possibility to generate energetic ions with ICRH has been proposed theoretically [16] and observed indirectly in experiments [17]. A distinct feature of this three-ion minority (TIM) heating scenario is the high efficiency of the power absorption at a very low concentration of the resonant ions. As a result, the minority ions can be accelerated to higher energies than in commonly used heating scenarios. Here we consider one of the possible TIM scenarios in ITER [16], and compare the transport properties of the heated minority to that of the alpha particle transport in a similar DT discharge. The strong non-Maxwellian feature of the energetic trace species is taken into account in our gyrokinetic analysis. We find that although turbulence advects these trace species in a similar way – apart from minor differences due to ionic composition effects – their transport properties can be very different because of differences in their distribution function. Alphas tend to transport outwards in steady state, while turbulence acts to accumulate the heated minorities in the region where the power absorption is the strongest.

Besides its relevance in fusion, the transport of high energy (and non-Maxwellian) minority species is also of interest in space- and astrophysics context. For instance, in the solar wind plasma the effective temperature of various ions have been observed to increase linearly or stronger with atomic mass [18], which may be a result of turbulent heating of heavy ions [19] in this highly collisionless environment. The methods and some of the results, presented here are also relevant in such circumstances.

The remainder of this paper is organized as follows. In Sec. 2 we discuss the heating scenario considered, and explain the modeling of the distribution function of the heated species. Sec. 3 starts with general considerations on how the turbulent transport of a trace species is treated, which is followed by the setup of the gyrokinetic simulations in Sec. 3.1. Then we present some general observations for the transport of a hot species in Sec. 3.2, before getting to the main results: comparing the transport of heated minorities with that of alpha particles in Sec.3.3. Finally we conclude in Sec. 4.

## 2. Scenario and properties of the heated species

We are interested in to what extent the transport of alpha particles in DT plasmas can be mimicked by that of heated minority ions in plasmas with different ion composition, but

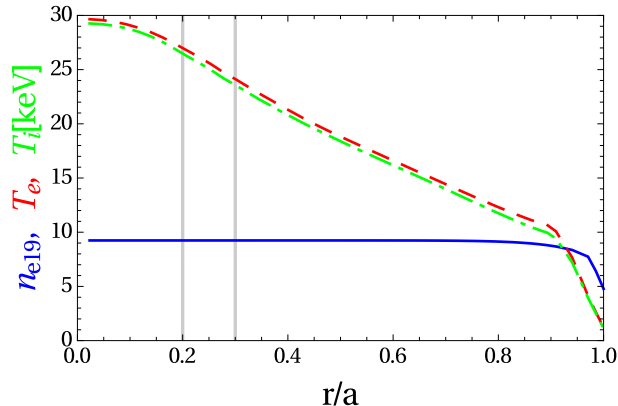


**Figure 1.** Density ( $n_e$  in  $10^{19} \text{ m}^{-3}$ , solid curve) and temperature profiles ( $T_e$  and  $T_i$  in keV, dashed and dash-dotted curves, respectively) in the projected ITER discharge 20020100. The radial region studied is indicated by the vertical bars.

similar profiles. In particular, we consider a non-activating ion composition: hydrogen (69.8% of electron density) and helium-4 (15%), with helium-3 (0.1%) minority as the heated species. The choice of the profiles is based on projected profiles in an ITER scenario simulation [20]. The profile data was accessed from the International Multi-tokamak Confinement Profile Database. We choose a high  $\beta_N$  hybrid [21] discharge (20020100), the temperature and electron density profiles of which are shown in Fig. 1. The profiles represent the self-consistent solution of an interpretative transport analysis using the PTRANSP code [22], as detailed in the Appendix of Ref. [20]. We kept the electron density, and assumed the concentration of the different ion species to be constant. Furthermore, some separation of the bulk ions might occur due to mass and charge effects on their turbulent transport [23, 24], and also modifications of the magnetic equilibrium when moving between the different ion composition cases, but these changes are not expected to qualitatively affect our results.

For our baseline study we will use the same temperature profiles and electron density profile as in the projected DT discharge. In the non-burning phase of ITER it is unlikely that such temperatures could be reached, but we will show in Sec. 3.3 that the energy dependence of the radial transport remains similar apart from scaling with the bulk temperature. In the simulations the hot minority is assumed to have a radially constant concentration, unless stated otherwise, and have distribution functions unaffected by the energy dependence of the radial transport.

The location of the ICRH resonance affects the achievable effective minority temperature. More central location leads to hotter minorities due to the absorption being localized to a smaller volume. Therefore generating energetic ions with central heating requires less ICRH power and may be advantageous to use in an experiment. However, here we choose a somewhat off-axis resonance location to assist our gyrokinetic study. Gyrokinetic simulations often fail to predict a finite turbulent transport close to

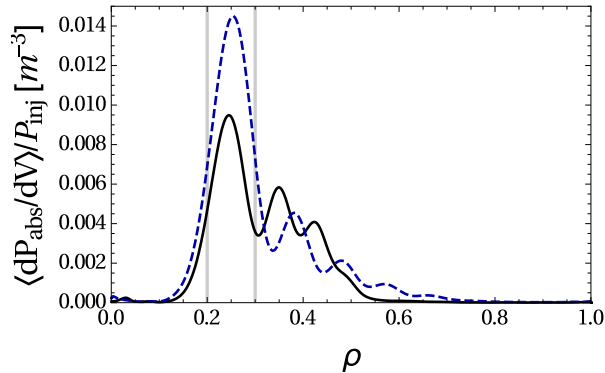


**Figure 2.** Flux surface averaged RF power density per injected power [ $\text{MW}/(\text{m}^3\text{MW}_{\text{inj}})$ ], absorbed by  $^3\text{He}$  ions; from TORIC simulations. Solid curve: at baseline profiles (shown in Fig. 1); dashed curve: at reduced temperature and density (profiles scaled from those in Fig. 1, corresponding to  $T_i(0) = 4\text{keV}$  and  $n_e(0) = 6 \cdot 10^{19}\text{m}^{-3}$ ). Note the different scales.

the magnetic axis (see for instance [25]), while some level of turbulent transport would be needed to predict temperature profiles consistent with the experiment. Without going into the discussion of possible reasons for this observation of turbulence simulations, we simply note that it is advantageous to choose a resonance location tangential to a flux surface where microinstabilities with positive growth rates were present in order to get a finite level of turbulent fluxes in the simulation. Accordingly, we choose the cyclotron resonance of  $^3\text{He}$  ions to be tangential to the  $\rho = 0.3$  flux surface from the outboard side ( $\rho = r/a$  is the normalized radius,  $r$  is the radial coordinate defined as the half width of the flux surface at the elevation of its centroid, and  $r = a$  at the last closed flux surface). For this resonance location and an on-axis toroidal field of  $B_T = 5.3\text{T}$  the RF source should operate at the frequency  $f_{\text{ICRH}} = 50\text{MHz}$ . A single toroidal wave number  $n_{\text{tor}} = 27$  representative for  $[0, 0, \pi, \pi]$  phasing of the ITER ICRH antenna [26, 27] is used in the simulations.

The flux surface average absorbed power density per unit injected power for  $^3\text{He}$  ions computed with the TORIC code [28, 29] is represented by the solid curve in Fig. 2. The simulations were made for the baseline plasma parameter profiles, assuming Maxwellian distributions for all particle species, and an effective temperature of  $1\text{MeV}$  for  $^3\text{He}$ . The heating modeling does not account for finite orbit width effects and does not evolve the distribution functions and the power deposition self-consistently. While a detailed ICRH modeling is outside the scope of our conceptual study, we note that such effects may lead to radial power deposition profiles which are considerably smoother, corresponding to possibly less sharp variations in the effective temperature of the heated minority. The importance of the relative magnitude of the density and temperature gradients of the hot species is discussed in Sec. 3.3.

A similar calculation for reduced temperatures and electron density is represented by the dashed curve in Figure 2; the profiles are re-scaled so that the central ion temperature

and electron density are  $T_i(0) = 4 \text{ keV}$  and  $n_e(0) = 6 \cdot 10^{19} \text{ m}^{-3}$ , respectively. In this case, when the bulk is colder, electron absorption is not efficient and almost 100% of the coupled power is absorbed by the  $^3\text{He}$  ions. For the baseline case, 23% of the launched power is absorbed by electrons with a radially broad absorption profile at the low field side. To reach similar minority-to-bulk temperature ratios in the studied radial region, we assume different injected ICRH powers:  $P_{\text{inj}} = 15 \text{ MW}$  in the baseline case and  $P_{\text{inj}} = 10 \text{ MW}$  for the re-scaled profiles.

The ICRH produces anisotropic minority distributions with a perpendicular-to-parallel temperature ratio larger than unity. However, with our gyrokinetic tool we can only model an isotropic species. This simplification is expected to have some effect on the energy dependent particle fluxes. It has been shown [30, 31] that, in electrostatic turbulence, at very high energies  $E$  the radial diffusivity of particles scale as  $E^{-3/2}$  for most of the particles except those with  $|v_{\parallel}|/v$  very close to 1. (We introduced the particle speed  $v = |\mathbf{v}|$  and the parallel velocity  $v_{\parallel} = \mathbf{v} \cdot \mathbf{b}$ , where  $\mathbf{v}$  is the particle velocity, and  $\mathbf{b} = \mathbf{B}/B$ , with  $B = |\mathbf{B}|$  and  $\mathbf{B}$  the unperturbed magnetic field.) Therefore, at least in the high energy limit, the transport of an RF heated anisotropic temperature species and an isotropic species with the same effective temperature is expected to scale similarly. However, at energies only a few times the bulk temperature (where most of the turbulent transport occurs) the pitch-angle dependence of the transport is non-trivial: at different energy ranges it can be weighted towards small or large pitch angles [32].

For the non-fluctuating distribution function  $f_{m0}(v, \rho)$  in the gyrokinetic modeling we use a simple isotropic analytical model derived by Stix, given by Eq. (33) of Ref. [33].  $f_{m0}$  depends on radius  $\rho$  through the spatial variation of the absorbed power density, and the densities and temperatures of the various non-trace particle species.

By using a non-fluctuating distribution function that is derived by balancing collisions and quasilinear diffusion due to the interaction with the RF waves means that we implicitly assume that the radial transport does not affect the distribution function. In reality the collisional slowing-down time and the radial turbulent transport time can compete at certain energies. The study of such non-perturbative effects is outside the scope of the present paper.

### 3. Turbulent transport

We calculate the turbulent transport of the heated minorities using radially local, electrostatic, nonlinear turbulence simulations using the “alphas” branch [34] of the gyrokinetic code GS2[35, 36]. This code is capable of handling a species with a non-fluctuating distribution which is isotropic but non-Maxwellian. We will assume the heated species to be present in trace quantities in the sense that it does not affect the turbulence. For electrostatic simulations of alpha particles the trace approximation was shown to be justified in Refs. [37, 12], although suprathreshold pressure gradients have recently been observed to have an effect in some electromagnetic simulations [38].

A trace species is passively advected by the turbulence and it does not affect the potential fluctuations, thus, given the fluctuation field, the gyrokinetic equation for such species is linear in the driving gradients in the distribution function. Consequently the fluxes in velocity space and configuration space are also linear in these gradients which may be utilized to calculate the fluxes for an arbitrary distribution function as shown in Ref. [14], and outlined below. Here we are only concerned with the radial transport, thus it is instructive to define the energy dependent radial particle flux as

$$\Gamma(E) = \left\langle \sum_{\sigma} \int \frac{\pi B d\lambda}{\sqrt{1 - \lambda B}} h_m \langle \mathbf{v}_{\mathbf{E}} \rangle_{\mathbf{R}_m} \cdot \nabla \rho \right\rangle_{t,\rho}, \quad (1)$$

where  $\mathbf{v}_{\mathbf{E}}$  is the fluctuating  $E \times B$  velocity,  $h_j = f_j - f_{j0} - e_j \phi \partial_E f_{j0}$  is the non-adiabatic perturbed distribution of the trace species that is characterized by its total distribution  $f_j$  and non-fluctuating distribution  $f_{j0}$  (not necessarily a Maxwellian), with  $\phi$  denoting the fluctuating electrostatic potential, and  $\partial_E$  the partial derivative with respect to the kinetic energy  $E (= m_j v^2/2)$ . Furthermore,  $\lambda = \mu/E$  with the magnetic moment  $\mu = m_j v_{\perp}^2/(2B)$ ,  $v_{\perp}^2 = v^2 - v_{\parallel}^2$ , and  $e_j$  and  $m_j$  are the charge and the mass of species  $j$ , respectively. The summation is done over the sign of the parallel velocity,  $\sigma$ , and  $\langle \cdot \rangle_{\mathbf{R}_j}$  represents a gyro-average holding the guiding center of the species  $\mathbf{R}_j$  fixed, while  $\langle \cdot \rangle_{t,\rho}$  is an average over the flux surface and a timescale much longer than the decorrelation time of turbulent structures. Physically Eq. (1) describes the net flux of particles across a flux surface at a given energy due to  $E \times B$  drift in the fluctuating electrostatic field. The total particle and heat fluxes are calculated as  $\{\Gamma_j, Q_j\} = \sqrt{2} m_j^{-3/2} \int dE \sqrt{E} \Gamma_j(E) \{1, E\}$ . The non-adiabatic distribution is calculated from the gyrokinetic equation, which, for species  $j$  reads

$$\begin{aligned} & \frac{\partial h_j}{\partial t} + (v_{\parallel} \mathbf{b} + \mathbf{v}_d + \langle \mathbf{v}_{\mathbf{E}} \rangle_{\mathbf{R}_j}) \cdot \nabla h_j - C[h_j] \\ & = -e_j \frac{\partial \langle \phi \rangle_{\mathbf{R}_j}}{\partial t} \frac{\partial f_{j0}}{\partial E} - \langle \mathbf{v}_{\mathbf{E}} \rangle_{\mathbf{R}_j} \cdot \nabla f_{j0}, \end{aligned} \quad (2)$$

where  $\mathbf{v}_d$  is the magnetic drift velocity,  $C$  is a gyroaveraged collision operator [39, 40]. The perturbed potential is calculated from the quasineutrality condition, but since a trace species does not contribute to the charge density,  $\phi$  is independent of  $f_m$  and thus for such species the problem is linear in  $h_m$ , as well as the drives  $\partial_E f_{m0}$  and  $\nabla f_{m0}$ . Consequently the radial particle flux is also linear in these drive terms

$$\Gamma_m(E) = -D_E \frac{\partial f_{m0}}{\partial E} - D_{\rho} \frac{\partial f_{m0}}{\partial \rho}, \quad (3)$$

where  $D_E$  and  $D_{\rho}$  are energy dependent transport coefficients. For a minority species with given charge and mass, these quantities are determined by the properties of the turbulence, which in turn only depends on the magnetic geometry and plasma parameter profiles of the non-trace species. Given two appropriately chosen distribution functions  $f_{m0}^{(1)}$  and  $f_{m0}^{(2)}$  corresponding to fluxes  $\Gamma_m^{(1)}$  and  $\Gamma_m^{(2)}$ , the resulting linear system can be inverted to obtain the transport coefficients. In particular, these distributions can be Maxwellians

with different radial gradients (chosen so that the linear problem is not singular across the energy range of interest) [14]; this is the approach we take. Once the transport coefficients are calculated  $\Gamma_m$  can be calculated from (3) for any  $f_{m0}(E, \rho)$ .

### 3.1. Gyrokinetic modeling

In the following we detail the gyrokinetic modeling using GS2 to obtain  $\Gamma_m(E)$ . We perform radially local simulations about the radial location  $\rho = 0.25$ , which is very close to the location where the power absorption of  $^3\text{He}$  is the highest in the cases shown in Fig. 2.

The simulations include two bulk ion species, (kinetic) electrons and two hot Maxwellian species in trace amounts which are of the same ion type but have different gradients. The latter are used to calculate the transport coefficients in (3) as described above. For the heated minority case the bulk ions are H (70%) and He (15%), and the trace species is  $^3\text{He}$ . For the alpha particle case the bulk species are D(50%), T (50%) and the trace species of  $^4\text{He}$ . The most important local magnetic geometry and plasma parameters at this position are the following: The safety factor  $q = 1.27$ , the magnetic shear  $s = 0.125$ , the aspect ratio  $R/a = 3.29$ , the elongation  $\kappa = 1.4$  and  $d\kappa/d\rho = 0.09$ , the triangularity  $\delta = 0.075$  and  $d\delta/d\rho = 0.14$ ,  $a^{-1}dR/d\rho = -0.08$ . Furthermore for all non-trace species  $a/L_{nj} \equiv -d(\ln n_j)/d\rho = 0$ , for the bulk ions  $a/L_{Ti} \equiv -d(\ln T_i)/d\rho = 1.509$ , for electrons  $a/L_{Te} \equiv -d(\ln T_e)/d\rho = 1.178$ , the temperature ratio is  $T_e/T_i = 1.02$ . In the simulations the normalized pressure  $\beta$  is set to 0. Collisions for bulk ions and electrons were accounted for using the conservative collision operator describing pitch angle scattering and energy diffusion [40].

The simulations used 28 grid points in extended poloidal angle covering one  $2\pi$  segment along the field line, the number of modes is 72 in the binormal ( $y$ ) direction and 48 in the radial ( $x$ ) direction with a domain size in both directions being 15 thermal Larmor radii of the first ion species (in some cases these numbers were increased to 96, 72 and 20, respectively). The number of untrapped pitch-angles moving in one direction along the field is 8 and the number of energy grid points is 24. The time step is  $0.1 a/v_1$  with  $v_j = v_1$  for the first ion species.

### 3.2. Fluxes against a temperature gradient

First we consider the total particle and energy transport of the heated  $^3\text{He}$  species across its region of strongest power absorption,  $\rho = 0.2 - 0.3$ . We assume that in terms of the transport of  $^3\text{He}$  the radial variations in the turbulence are weak compared to the changes in  $f_{m0}$ . This is reasonable when the power absorption varies much more rapidly than the background profiles (compare Figs. 1 and 2; in the studied region is indicated with the vertical bars). Thus we calculate the transport coefficients of Eq. (3) using a single local gyrokinetic simulation at  $\rho = 0.25$  and calculate how the fluxes vary due the radial variation of  $f_{m0}$ .



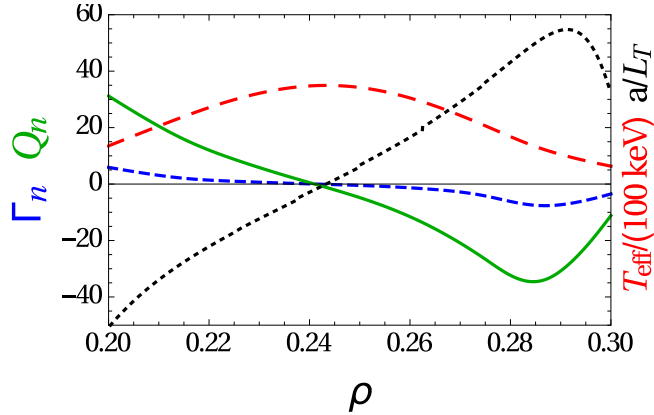


**Figure 3.** Total normalized turbulent particle- (dashed, blue curve) and energy (solid, green) fluxes of the heated minority across the region of strongest heat absorption. Absolute fluxes are given by  $\Gamma_m = \Gamma_n n_m v_r \rho_*^2$ ,  $Q_m = Q_n n_m v_r T_r \rho_*^2$ . The effective temperature of the minorities ( $T_{\text{eff}}$  in 100keV; red, long dashed) and the corresponding logarithmic temperature gradient ( $a/L_T = -d \ln T_{\text{eff}}/d\rho$ ; black, dotted) are also plotted. We assumed  $P_{\text{inj}} = 15$  MW and a power deposition profile shown with the solid line in Fig. 2. Note that positive fluxes are flowing radially outward, which means that both of the fluxes are flowing against the effective temperature gradient (the radial density gradient of the minorities is zero).

Figure 3 shows the normalized total particle- ( $\Gamma_n$ , dashed curve) and energy fluxes ( $Q_n$ , solid) of  ${}^3\text{He}$  as a functions of  $\rho$ , together with the effective temperature of the heated species ( $T_{\text{eff}} = n_m^{-1} \int d^3v (m_m v^2/3) f_{m0}$  given in 100 keV units, long dashed), and its logarithmic gradient  $a/L_T = -d(\ln T_{\text{eff}})/d\rho$ . The absolute fluxes are given by  $\Gamma_m = \Gamma_n n_m v_r \rho_*^2$ ,  $Q_m = Q_n n_m v_r T_r \rho_*^2$ , where  $T_r$ ,  $v_r$  and  $\rho_* = \rho_r/a$  are the reference temperature, reference thermal speed and normalized thermal Larmor radius, which are set to be those quantities for the first ion species (H). We note that, for the sharp absorption profile we consider the effective temperature varies on a rather small spatial scale. At  $\rho = 0.25$  a 3.5 MeV trapped  ${}^3\text{He}$  ion has a typical orbit width of  $0.08a$  making the local gyrokinetic treatment questionable for the most energetic ions. However, as we will show, most of the turbulent transport occurs at a suprathermal energy range of  $\sim 100$  keV, where the orbit width is significantly smaller,  $\sim 0.01a$ .

Following the radial variation of the absorbed power, the effective temperature peaks close to the flux surface  $\rho = 0.25$ . Notably, for our baseline parameters the effective temperature of the heated species exceeds 3 MeV (while it is expected to be lower for a less hot plasma). Even more remarkable is the fact that both the particle and the energy fluxes are flowing in the direction of the  $T_{\text{eff}}$  peak (note that radially outward fluxes are defined to be positive, and the density gradients are zero for all species). Particularly, the fluxes and  $a/L_T$  change sign at the same radial location.

The reason for both  $\Gamma_m$  and  $Q_m$  flowing against the driving temperature gradient – which might be puzzling for the first sight – is illustrated in Fig. 4. The energy

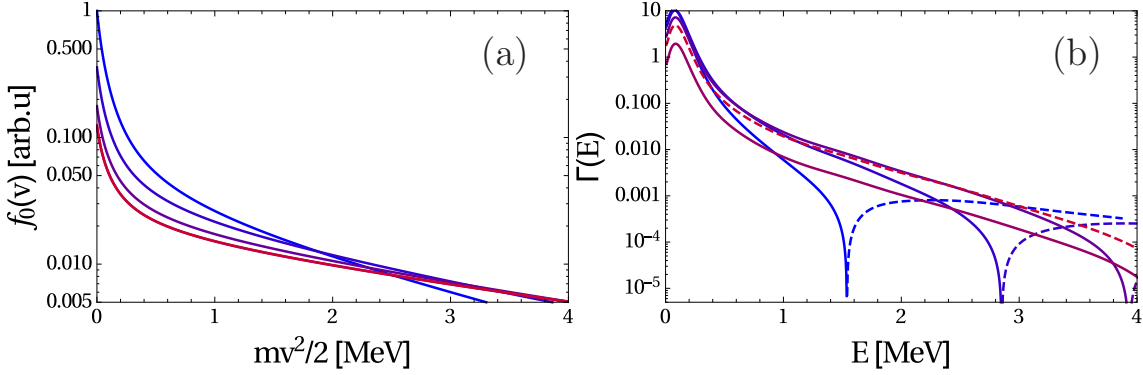


**Figure 4.** Energy variation of  $f_0(v)$  (a) and  $\Gamma(E)$  (b) at different radial locations close to the absorption peak. Dashed lines represent negative values. The color code varies from blue to purple shades with increasing radius;  $\rho$  changes on the scale  $\{0.2, 0.2125, 0.225, 0.2325, 0.25\}$ . In (a) the  $\rho = 0.2325$  and  $0.25$  curves, located just below and above the effective temperature maximum, overlap almost completely, while the fluxes in those locations have opposite sign, as seen in (b).

dependence of the distribution function  $f_0$  is shown for various radii in Fig. 4a moving from  $\rho = 0.2$  to  $0.25$ , approaching the  $T_{\text{eff}}$  peak and passing its maximum slightly at the last location (henceforth the species subscript for the hot trace species is suppressed). The normalization preserves the relative magnitude of the distributions (i.e. their number density is radially constant). The effective temperature increases as the peak is approached radially – while the  ${}^3\text{He}$  density remains constant – causing the distribution function to spread out towards larger energies and become depleted at low energies. The corresponding  $\Gamma(E)$  functions are plotted in Fig. 4b (with similar color coding for the different radii; dashed lines representing negative values). The energy dependent fluxes have a maximum at very low energy ( $\sim 100$  keV) compared to the typical effective temperatures ( $\sim$  MeV) and they decay rapidly due to FLR effects. The fluxes are thus dominated in an energy range where the distribution function is depleted when moving radially towards the higher temperature region. In the light of these observations fluxes towards the peak of the  $T_{\text{eff}}$ , shown in Fig. 3, is not surprising:  $f_0(E \sim 100 \text{ keV}, \rho)$  has a minimum at the radius of the highest  $T_{\text{eff}}$ .

It is clear that the phenomena is not the result of the  $f_0$  being non-Maxwellian. Figure 5a shows the normalized particle and heat fluxes (dashed and solid lines, respectively) as functions of the temperature of a Maxwellian trace species. We assume that the turbulence properties in terms of  $D_E$  and  $D_\rho$  are the same as for our baseline case (detailed in Sec. 3.1), with  $T_r = 25$  keV,  $a/L_{Tm} = -30$ , and  $a/L_{nm} = 0$ . For  $a/L_{Tm} < 0$  (minority temperature increases with radius) we normally expect an inward heat flux  $Q_n < 0$ ; indeed when  $T_m \sim T_r$  both  $Q_n$  and  $\Gamma_n$  are negative. However, as  $T_m$  is increased first the particle then the heat flux change sign opposing the minority temperature gradient. Radial fluxes in the presence of gradients represent sources in the local free energy balance equation (see [41] and references therein). As a trace species

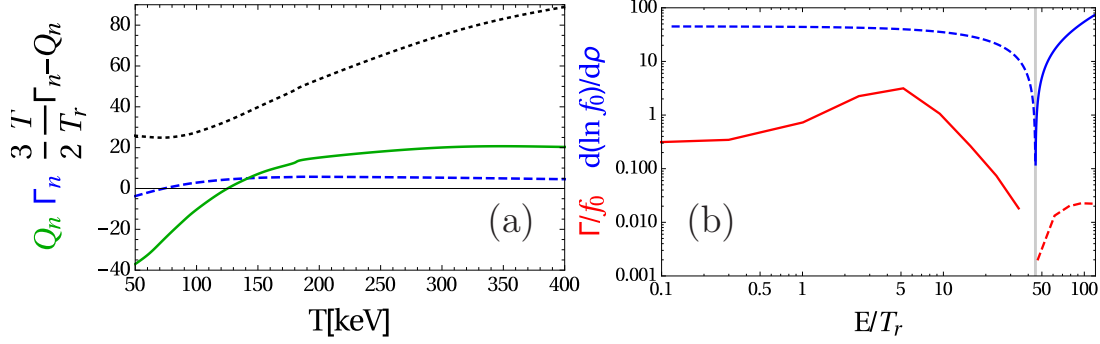


**Figure 5.** Radial fluxes of a high temperature Maxwellian trace. (a) Total normalized particle- (blue, dashed curve) and energy (green, solid) fluxes as functions of the minority temperature,  $T$ . A quantity related to the entropy production by radial fluxes in this scenario (temperature profile peaks outward, density gradient zero) is also plotted (black, dotted). Note that while the fluxes change sign with increasing minority temperature, the entropy production always stays positive. (b)  $\Gamma(E)$  (red, lower curve) and  $d(\ln f_0)/d\rho$  (blue, upper curve) as functions of energy for a fixed minority temperature ( $T/T_r = 30$ ). Both quantities change sign at the same energy (dashed curves represents negative values), thus at a given energy the flux is not flowing against the radial gradient.

does not exchange energy with the fields the free energy is conserved for the species in isolation, and destroyed only by collisions (however small the collision frequency may be). Therefore negative free energy generation would imply negative entropy production that is unphysical. This problem does not arise in our case, since – for zero gradients of density and toroidal rotation frequency, and  $a/L_{T_m} < 0$  – the free energy generation by the fluxes is proportional to  $(3/2)\Gamma_m T_m - Q_m \propto (3/2)\Gamma_n T_m/T_r - Q_n$ . This quantity remains positive even though the fluxes change signs with increasing  $T_m$  as shown by the dotted curve in Fig. 5a. Considering the energy dependence of the radial flux and the radial gradient (shown by red and blue curves in Fig. 5b, respectively; negative values are represented by dashed lines) reveals that the radial flux indeed flows down the radial gradient at a given energy (the two quantities have opposite signs and change sign together). In this case the radial fluxes are dominated by the contribution from an energy range  $E/T_r \approx 5$ , where the distribution function is decreasing radially, while  $dT_m/dr$  increases.

### 3.3. Transport of heated species and alphas

Finally, we turn our attention to the radial transport of the hot minorities and compare the results for the heated impurities and alpha particles. We consider the radial location  $\rho = 0.275$ , somewhat outside the maximum of the RF power deposition so that the effective temperature of  $^3\text{He}$  decreases radially while it is still very high ( $T_{\text{eff}} \approx 2.8 \text{ MeV}$ ).

Assuming similar background profiles (discussed in Sec. 2) but different ion composition results in qualitatively similar turbulent transport in terms of the transport coefficients for a trace species. The transport coefficients  $D_E$  (dashed curves, given in units of  $\rho_*^2 v_r T_r$ ) and  $D_\rho$  (solid curves, in units of  $\rho_*^2 v_r$ ) are shown for alpha particles (blue

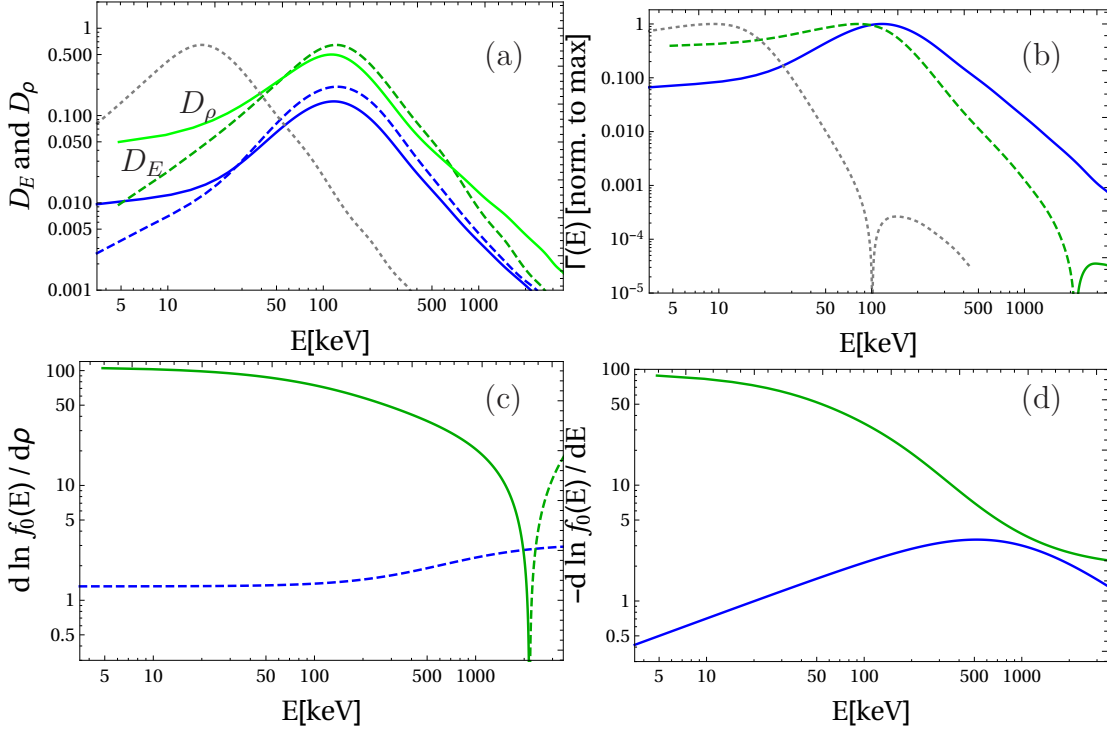


**Figure 6.** Energy dependent transport coefficients (a), radial particle flux (b), and logarithmic energy- (c) and radial (d) derivatives of the distribution functions of the energetic minority. The calculations are based on the 20020100 ITER discharge at  $\rho = 0.275$ . Blue curves:  $\alpha$  slowing-down distribution,  $\alpha$ -source and turbulence calculated for 50 – 50% D-T. Green curves: heated  $\text{He}^3$ , ion composition and heating of Fig. 2 (solid line). Dashed lines represent negative values. Dotted lines show results for the reduced density and temperature plasma corresponding to the dashed curve of Fig. 2; these are  $|D_E|$  in (a) and  $|\Gamma|$  in (b).

curves, D-T plasma) and heated  $^3\text{He}$  (green curves, H-He plasma) in Fig. 6a. In terms of their energy dependence, both quantities peak around 100 keV and decay towards high energies due to FLR effects. The radial coefficient  $D_\rho$  is positive, as it should be for positive entropy generation. The energy coefficient  $D_E$  is negative, similarly to the findings of Ref. [42]. It being negative means that without radial variations in the distribution function there would be inward fluxes (except for distributions non-monotonic in energy), which can be thought as a generalized pinch due to the background turbulence, driven by gradients in the distribution of the bulk species. However,  $D_E \partial_E f_0 \ll D_\rho \partial_\rho f_0$ , that is, in terms of  $\Gamma(E)$  the radial variation of the distribution function at a given energy is more important than its energy variation. This is expected for a hot species with radial gradients comparable to, or larger than, those of the bulk [10]: Although the diamagnetic frequency of the bulk species is comparable to the characteristic mode frequency of the underlying drift waves, the diamagnetic frequency of the hot species – ultimately giving rise to the  $D_\rho \partial_\rho f_0$  contribution – is typically much higher than the mode frequency. The transport coefficients of the heated  $^3\text{He}$  are approximately 3 times larger

in absolute magnitude than those of the alpha particles, due to differences in the bulk ion composition. However, this difference merely reflects a change in the turbulence intensity: a similar difference in the total ion heat fluxes is also observed. These simulations are gradient driven and exhibit a stiff ion heat transport; in an experiment the gradients would slightly adjust to produce a fluctuation amplitude and a heat flux as required by the sources. Thus, for a similar heating power inside the flux surface of interest we expect the magnitude of the transport coefficients to be very similar in the two plasmas.

As we have established that turbulence has a similar effect on the hot species in both plasmas, any notable differences in terms of their radial transport should come from differences in their distribution functions. The generation mechanism of the hot species is fundamentally different: while alpha particles are born at high energy with a radially varying source and slow down due to collisions, the distribution of the heated species is shaped by a quasilinear diffusion due to the interaction with the electromagnetic field and collisions. In particular, if we could instantaneously “switch on” D-T fusion, alpha particles would start filling up phase space from high energy, while when RF heating is switched on the distribution expands from lower towards higher energies. Naturally, the hot alpha particle distributions have a radial density variation due to the source gradients, while the heated distribution can have a potentially strong effective temperature gradient depending on the power deposition profile.

With time the fluxes in phase-space would become divergence free as the minorities would settle at some equilibrium distribution function (analogous to the converged plasma parameter profiles in predictive modeling). In our gradient driven modeling we cannot address this question, and we are only concerned with the fluxes for given distribution functions. The radially decreasing source strength of alphas and the radially decreasing effective temperature thus clarifies  $d(\ln f_0)/d\rho$  being negative for alphas for all energies, and being large and positive for  $^3\text{He}$  over most of the energy range considered, as shown in Fig. 6c.

The energy derivatives are shown in Fig. 6d. The high and low energy limits of the  $^3\text{He}$  distribution are different temperature Maxwellians thus  $-d(\ln f_0)/dE$  varies between two constant asymptotes, while this quantity for the alpha slowing down distribution is non-monotonic with a peak comparable to the critical energy (the He ash distribution is not considered). The resulting energy dependent fluxes normalized to their maximum values are shown in Fig. 6b. For the heated  $^3\text{He}$  both the energy and the radial gradient drive terms cause inward fluxes, thus the total fluxes are inward. A sign change of  $\Gamma(E)$  occurs near where  $d \ln f_0(E)/d\rho$  changes sign, but above that energy  $\Gamma(E)$  is so small that the total particle and energy fluxes remain negative. This would, on longer time scales, lead to an accumulation of the heated species around the maximum of the power absorption. While the energy derivative contribution is negative for the alphas too, the radial gradient driven part is positive for them, producing outward total flux.

After considering a completely flat minority density profile and a rather sharp effective temperature variation in our heated minority example, now we consider the

effect of these assumptions being relaxed. At the radial location  $\rho = 0.275$  the effective temperature gradient is  $a/L_T = 35.6$ , which is due to a comparably large gradient in the absorption profile  $a/L_P \equiv -d(\ln P_{\text{abs}})/d\rho = 23$ . Reducing  $a/L_T$  at zero density gradient linearly scales down the fluxes, and their sign is unaffected. However, when the minority has a density gradient comparable to the effective temperature gradient, the fluxes can change sign. In our heated minority example, if  $T_{\text{eff}}$  and  $a/L_T$  are held fixed  $\Gamma_m (Q_m)$  is found to change sign at a logarithmic minority density gradient of  $a/L_n = 48$  ( $a/L_n = 28$ ). If the absorption profile is held fixed then the sign change happens at lower density gradients,  $a/L_n = 18$  ( $a/L_n = 13.5$ ), since then the density variation also affects the effective temperature variation.

Although we do not evolve the distributions of the hot trace species towards a steady state, we note that such task is feasible for alpha particles, and has been done with the T3CORE code presented in Ref. [14, 43]. For alphas the steady state is determined by the sources, the slowing down and the radial transport due to turbulence; the generation through fusion should be balanced by the total radial transport. The heated species problem is considerably more involved, since the process of the heating itself depends on the heated distribution function, we do not attempt to tackle this very challenging problem here.

For the  $^3\text{He}$  heating case we have shown simulation results with plasma parameters similar to a projected ITER DT discharge (Case 1). Although the similarity of the plasma parameter profiles was convenient in simplifying the comparison, the densities and temperatures in a non-activated phase discharge relevant for a TIM heating experiment could be significantly lower. To assess corresponding differences in the transport we calculate the transport coefficients and the radial flux of the heated species for densities and temperatures scaled by constant factors (see caption for Fig. 2, Case 2). Also, we reduce the injected power to  $P_{\text{inj}} = 10$  MW, since the power absorption by the  $^3\text{He}$  ions is more effective at the reduced bulk temperatures.

The local gyrokinetic simulation results are only affected by these parameter changes through changes in collisionality (besides changes in the normalization, which do not enter the simulation). The collisionality in this ion temperature gradient mode driven turbulence has only minor effects. The transport coefficients are thus similar, apart from a shift in the energy range by a factor 7.3 that is the same as the ratio between the temperatures in Case 1 and Case 2. For comparison we show  $|D_E|$  for Case 2 in 6a, which is to be compared with the green dashed line for Case 1. Due to the change in collisionality the heated distribution in Case 2 is not simply down-shifted in energy but it is slightly different, which leads to that  $\Gamma(E)$  is visibly different between the two cases (see  $|\Gamma(E)|$  plotted with dotted line in 6b), with the ratio between the peak energies being 11.2 and the ratio between the energies where the sign change occurs is 21.4. The qualitative behavior and the sign of the total fluxes remain the same.

## 4. Conclusions

We have studied the turbulent transport properties of various energetic, non-Maxwellian trace species in magnetized plasmas. In particular we compared the radial transport of the hot species in the three ion minority ICRH scheme (assuming a peaked off-axis power deposition) to that of alpha particles based on projected ITER plasma parameter profiles. The motivation for such comparison is the prospect of mimicking alpha particle confinement with MeV range ions already in the non-activated phase of ITER operation, or in present day experiments.

As a general observation, we find that a species (Maxwellian or not), characterized by an effective temperature much higher than the bulk temperature and an effective temperature gradient sufficiently higher than the density gradient, can develop energy and particle fluxes flowing against the gradients. The reason is that most of the turbulent transport occurs on an energy range comparable with the bulk temperature, and it is FLR-suppressed towards high energies. A temperature gradient for such a high temperature species corresponds to a radial gradient of the distribution function with the opposite sign at these energies much lower than the species' effective temperature. The behavior of heated minorities is governed by this phenomena. For minorities much hotter than the bulk plasma the use of energy dependent radial particle flux is more informative than the total particle and heat fluxes.

We find that the energy dependent turbulent transport coefficients of the passively advected species are similar in the different ion configurations considered (H-He plasma with a trace  $^3\text{He}$  and D-T plasma with trace alphas). The radial turbulent transport is dominated by a contribution from a suprathermal energy range,  $\sim 100$  keV for the ITER-relevant bulk temperatures considered. However, the radial particle transport is different because of differences between the distribution functions of the hot species. The alphas have a radially varying particle source corresponding to a radially decreasing density, which necessarily corresponds to an outward total particle transport in steady state. The heated minorities, if they originally have a density profile less steep than the effective temperature profile, will be radially transported towards the region where most of the RF heat deposition takes place, as their distribution function is depleted there across the energy ranges dominating the turbulent transport. These results suggest that their steady state density profile should be peaked in the region where the heat deposition is the strongest. Despite the observed differences in their turbulent transport, by generating ions in the right energy range in a controllable fashion, the TIM scheme would still be very useful in validating alpha particle transport prediction tools before the activated phase of the ITER operation. Our results point out the importance of these tools to account for effects stemming from the differences in alpha and heated minority distribution functions.

## Acknowledgments

The authors are grateful to P. Helander, A. Schekochihin and I. Abel for fruitful discussions, and to M. Brambilla and R. Bilato for providing the TORIC code. This work was supported by the International Career Grant (Dnr. 330-2014-6313) and the Framework grant for Strategic Energy Research (Dnr. 2014-5392) from Vetenskapsrådet, and the US DoE grants DEFG0293ER54197 and DEFC0208ER54964. The gyrokinetic simulations were performed on Hopper at NERSC, and on Hebbe at C3SE (project nr. SNIC2016-1-161).

## References

- [1] ITER Physics Expert Group on Energetic Particles H, Drive C and Editors I P B 1999 *Nuclear Fusion* **39** 2471 URL <http://stacks.iop.org/0029-5515/39/i=12/a=305>
- [2] Fasoli A, Gormenzano C, Berk H, Breizman B, Briguglio S, Darrow D, Gorelenkov N, Heidbrink W, Jaun A, Konovalov S, Nazikian R, Noterdaeme J M, Sharapov S, Shinohara K, Testa D, Tobita K, Todo Y, Vlad G and Zonca F 2007 *Nuclear Fusion* **47** S264 URL <http://stacks.iop.org/0029-5515/47/i=6/a=S05>
- [3] Mantsinen M J, Mayoral M L, Kiptily V G, Sharapov S E, Alper B, Bickley A, de Baar M, Eriksson L G, Gondhalekar A, Hellsten T, Lawson K, Nguyen F, Noterdaeme J M, Righi E, Tuccillo A A and Zerbini M 2002 *Phys. Rev. Lett.* **88**(10) 105002 URL <http://link.aps.org/doi/10.1103/PhysRevLett.88.105002>
- [4] Pizzuto A, Gnesotto F, Lontano M, Albanese R, Ambrosino G, Apicella M, Baruzzo M, Bruschi A, Calabr G, Cardinali A, Cesario R, Crisanti F, Cocilovo V, Coletti A, Coletti R, Costa P, Briguglio S, Frosi P, Crescenzi F, Coccoresse V, Cucchiario A, Troia C D, Esposito B, Fogaccia G, Giovannozzi E, Granucci G, Maddaluno G, Maggiora R, Marinucci M, Marocco D, Martin P, Mazzitelli G, Mirizzi F, Nowak S, Paccagnella R, Panaccione L, Ravera G, Orsitto F, Ridolfini V P, Ramogida G, Rita C, Santinelli M, Schneider M, Tuccillo A, Zagrski R, Valisa M, Villari R, Vlad G and Zonca F 2010 *Nuclear Fusion* **50** 095005 URL <http://stacks.iop.org/0029-5515/50/i=9/a=095005>
- [5] Lackner K, Coster D and Schneider R 1998 *Czechoslovak Journal of Physics* **48** 167–175
- [6] Romanelli F, Coletti A, Gormezano C, Lucci F, Pizzuto A, Righetti G B, Group T F and Group T E 2004 *Fusion Science and Technology* **45** 483 URL [http://www.ans.org/pubs/journals/fst/a\\_526](http://www.ans.org/pubs/journals/fst/a_526)
- [7] Calabr G, Crisanti F, Ramogida G, Albanese R, Cardinali A, Cucchiario A, Granucci G, Maddaluno G, Marinucci M, Nowak S, Pizzuto A, Ridolfini V P, Pironti A, Tuccillo A and Zonca F 2009 *Nuclear Fusion* **49** 055002 URL <http://stacks.iop.org/0029-5515/49/i=5/a=055002>
- [8] Tobita K, Nakayama T, Konovalov S V and Sato M 2003 *Plasma Physics and Controlled Fusion* **45** 133 URL <http://stacks.iop.org/0741-3335/45/i=2/a=305>
- [9] Gorelenkov N, Pinches S and Toi K 2014 *Nuclear Fusion* **54** 125001 URL <http://stacks.iop.org/0029-5515/54/i=12/a=125001>
- [10] Chen L and Zonca F 2016 *Rev. Mod. Phys.* **88**(1) 015008 URL <http://link.aps.org/doi/10.1103/RevModPhys.88.015008>
- [11] Pinches S D, Chapman I T, Lauber P W, Oliver H J C, Sharapov S E, Shinohara K and Tani K 2015 *Physics of Plasmas* **22** 021807 URL <http://scitation.aip.org/content/aip/journal/pop/22/2/10.1063/1.4908551>
- [12] Wilkie G J, Abel I G, Highcock E G and Dorland W 2015 *Journal of Plasma Physics* **81**(03) 905810306



- [13] Wilkie G J, Abel I G, Landreman M and Dorland W 2016 *Physics of Plasmas* **23** 060703 URL <http://scitation.aip.org/content/aip/journal/pop/23/6/10.1063/1.4953420>
- [14] Wilkie G J 2015 *Microturbulent transport of non-Maxwellian alpha particles* Ph.D. thesis University of Maryland, Department of Physics
- [15] Sigmar D, Gormley R and Kamelander G 1993 *Nuclear Fusion* **33** 677 URL <http://stacks.iop.org/0029-5515/33/i=5/a=I01>
- [16] Kazakov Y, Eester D V, Dumont R and Ongena J 2015 *Nuclear Fusion* **55** 032001 URL <http://stacks.iop.org/0029-5515/55/i=3/a=032001>
- [17] Wukitch S, Cziegler I, Kazakov Y, Labomard B, Lin Y, Ongena J, Perkins R, Terry J, Van Eester D, Wright J, A H, P E, Porkolab M and the Alcator C-Mod Team 2015 ICRF experiments in Alcator C-Mod *57th Annual Meeting of the APS Division of Plasma Physics* (Savannah, GA, USA) URL [http://www-internal.psfc.mit.edu/research/alcator/pubs/APS/APS2015/Wukitch\\_poster\\_APS-2015.pdf](http://www-internal.psfc.mit.edu/research/alcator/pubs/APS/APS2015/Wukitch_poster_APS-2015.pdf)
- [18] Schmidt W K H, Rosenbauer H, Shelly E G and Geiss J 1980 *Geophysical Research Letters* **7** 697–700 ISSN 1944-8007 URL <http://dx.doi.org/10.1029/GL007i009p00697>
- [19] Barnes M, Parra F I and Dorland W 2012 *Phys. Rev. Lett.* **109**(18) 185003 URL <http://link.aps.org/doi/10.1103/PhysRevLett.109.185003>
- [20] Roach C, Walters M, Budny R, Imbeaux F, Fredian T, Greenwald M, Stillerman J, Alexander D, Carlsson J, Cary J, Ryter F, Stober J, Gohil P, Greenfield C, Murakami M, Bracco G, Esposito B, Romanelli M, Parail V, Stubberfield P, Voitsekhovitch I, Brickley C, Field A, Sakamoto Y, Fujita T, Fukuda T, Hayashi N, Hogewij G, Chudnovskiy A, Kinerva N, Kessel C, Aniel T, Hoang G, Ongena J, Doyle E, Houlberg W, Polevoi A, Database I C, Group M T and Group I T P T 2008 *Nuclear Fusion* **48** 125001 URL <http://stacks.iop.org/0029-5515/48/i=12/a=125001>
- [21] Gormezano C, Sips A, Luce T, Ide S, Becoulet A, Litaudon X, Isayama A, Hobirk J, Wade M, Oikawa T, Prater R, Zvonkov A, Lloyd B, Suzuki T, Barbato E, Bonoli P, Phillips C, Vdovin V, Joffrin E, Casper T, Ferron J, Mazon D, Moreau D, Bundy R, Kessel C, Fukuyama A, Hayashi N, Imbeaux F, Murakami M, Polevoi A and John H S 2007 *Nuclear Fusion* **47** S285 URL <http://stacks.iop.org/0029-5515/47/i=6/a=S06>
- [22] Budny R, Andre R, Bateman G, Halpern F, Kessel C, Kritz A and McCune D 2008 *Nuclear Fusion* **48** 075005 URL <http://stacks.iop.org/0029-5515/48/i=7/a=075005>
- [23] Estrada-Mila C, Candy J and Waltz R E 2005 *Physics of Plasmas* **12** 022305 URL <http://scitation.aip.org/content/aip/journal/pop/12/2/10.1063/1.1848544>
- [24] Pusztai I, Candy J and Gohil P 2011 *Physics of Plasmas* **18** 122501 URL <http://scitation.aip.org/content/aip/journal/pop/18/12/10.1063/1.3663844>
- [25] Holland C, Candy J, Waltz R E, White A E, McKee G R, Shafer M W, Schmitz L and Tynan G R 2008 *Journal of Physics: Conference Series* **125** 012043 URL <http://stacks.iop.org/1742-6596/125/i=1/a=012043>
- [26] Budny R, Berry L, Bilato R, Bonoli P, Brambilla M, Dumont R, Fukuyama A, Harvey R, Jaeger E, Indireskumar K, Lerche E, McCune D, Phillips C, Vdovin V, Wright J and members of the ITPA-IOS 2012 *Nuclear Fusion* **52** 023023 URL <http://stacks.iop.org/0029-5515/52/i=2/a=023023>
- [27] Dumont R J 2009 *AIP Conference Proceedings* **1187**
- [28] Brambilla M 1999 *Plasma Physics and Controlled Fusion* **41** 1 URL <http://stacks.iop.org/0741-3335/41/i=1/a=002>
- [29] Bilato R, Brambilla M, Maj O, Horton L, Maggi C and Stober J 2011 *Nuclear Fusion* **51** 103034 URL <http://stacks.iop.org/0029-5515/51/i=10/a=103034>
- [30] Hauff T and Jenko F 2008 *Physics of Plasmas* **15** 112307 URL <http://scitation.aip.org/content/aip/journal/pop/15/11/10.1063/1.3013453>
- [31] Pueschel M, Jenko F, Schneller M, Hauff T, Gnter S and Tardini G 2012 *Nuclear Fusion* **52** 103018 URL <http://stacks.iop.org/0029-5515/52/i=10/a=103018>
- [32] Zhang W, Decyk V, Holod I, Xiao Y, Lin Z and Chen L 2010 *Physics of Plasmas* **17** 055902 URL

- <http://scitation.aip.org/content/aip/journal/pop/17/5/10.1063/1.3379471>
- [33] Stix T 1975 *Nuclear Fusion* **15** 737 URL <http://stacks.iop.org/0029-5515/15/i=5/a=003>
- [34] Wilkie G J 2015 alphas branch of the gyrokinetic code gs2 URL <https://svn.code.sf.net/p/gyrokinetics/code/gs2/branches/alphas/>
- [35] Kotschenreuther M, Rewoldt G and Tang W 1995 *Computer Physics Communications* **88** 128 – 140 ISSN 0010-4655 URL <http://www.sciencedirect.com/science/article/pii/001046559500035E>
- [36] Dorland W, Jenko F, Kotschenreuther M and Rogers B N 2000 *Phys. Rev. Lett.* **85**(26) 5579–5582 URL <http://link.aps.org/doi/10.1103/PhysRevLett.85.5579>
- [37] Angioni C and Peeters A G 2008 *Physics of Plasmas* **15** 052307 URL <http://scitation.aip.org/content/aip/journal/pop/15/5/10.1063/1.2913610>
- [38] Citrin J, Jenko F, Mantica P, Told D, Bourdelle C, Garcia J, Haverkort J W, Hogewij G M D, Johnson T and Pueschel M J 2013 *Phys. Rev. Lett.* **111**(15) 155001 URL <http://link.aps.org/doi/10.1103/PhysRevLett.111.155001>
- [39] Abel I G, Barnes M, Cowley S C, Dorland W and Schekochihin A A 2008 *Physics of Plasmas* **15** 122509 URL <http://scitation.aip.org/content/aip/journal/pop/15/12/10.1063/1.3046067>
- [40] Barnes M, Abel I G, Dorland W, Ernst D R, Hammett G W, Ricci P, Rogers B N, Schekochihin A A and Tatsuno T 2009 *Physics of Plasmas* **16** 072107 URL <http://scitation.aip.org/content/aip/journal/pop/16/7/10.1063/1.3155085>
- [41] Abel I G, Plunk G G, Wang E, Barnes M, Cowley S C, Dorland W and Schekochihin A A 2013 *Reports on Progress in Physics* **76** 116201 URL <http://stacks.iop.org/0034-4885/76/i=11/a=116201>
- [42] Waltz R E, Bass E M and Staebler G M 2013 *Physics of Plasmas* **20** 042510 URL <http://scitation.aip.org/content/aip/journal/pop/20/4/10.1063/1.4802808>
- [43] Wilkie G J 2015 T3core code URL <https://github.com/gjwilkie/t3core>